Published in final edited form as:
Nat Methods. 2014 January ; 11(1): 55–58. doi:10.1038/nmeth.2730.

Deciphering laminar-specific neural inputs with line-scanning fMRI

Xin Yu[*], **Chunqi Qian**, **Der-yow Chen**, **Stephen Dodd**, and **Alan P. Koretsky**[*]
Laboratory of Functional and Molecular Imaging, National Institute of Neurological Disorders and Stroke, National Institutes of Health, Bethesda, MD, 20892, USA

Abstract

Using a line-scanning method during functional magnetic resonance imaging (fMRI) we obtain high temporal (50 ms) and spatial (50 μm) resolution information along the cortical thickness, and show that the laminar position of fMRI onset coincides with distinct neural inputs t in therat somatosensory and motor cortices. This laminar specific fMRI onset allowed the identification of the neural inputs underlying ipsilateral fMRI activation in the barrel cortex due to peripheral denervation-induced plasticity.

The fMRI signal is indirectly coupled to neural activity by hemodynamic responses, such as increased blood flow, blood volume, and blood oxygenation. These hemodynamic changes are detected by fMRI techniques, such as Blood-Oxygen-Level-Dependent (BOLD) fMRI[1]. The correlation of neural activity with vascular changes has enabled the large-scale mapping of brain function using task-related or resting state fMRI protocols[2, 3]. These fMRI studies estimate connection strengths, based on signal-correlations, among brain regions, but do not reveal the specific neural circuitry underlying the fMRI signal. High field fMRI has pushed the spatial resolution of fMRI to the submillimeter range, which makes it possible to distinguish fMRI signals from a specific cortical column[4, 5] and identify specific features of laminar fMRI responses across the cortical thickness[6]. However, it remains challenging to use these laminar related fMRI signals to extract neural information about the underlying circuit.

Different temporal phases of the fMRI response may contain distinct information about the neural sources causing the hemodynamic signal[4, 7, 8]. The initial BOLD fMRI onset signal has been reported to be spatially associated with the neural activation event to a larger extent than the later phases[7, 9]. In the rat somatosensory cortex, the early positive BOLD fMRI signal has been shown to initiate in layer 4/5 in response to whisker/forepaw stimulation[9, 10]. This signal can be detected between 600–800 ms after the stimulus onset

[*]Correspondence: yuxin@mail.nih.gov and koretskya@ninds.nih.gov.

Competing financial interests
The authors declare no competing financial interests.

Author Contributions
X.Y. and A.P.K. conceived the line-scanning strategy and designed experiments. X.Y. established the line-scanning method, performed experiments, and analyzed the data. C.Q. and D.C. performed blind experiments on the MEMRI tracing and line-scanning fMRI of the plasticity model. S.D. provided MR technical support and IDL analytical tools. X.Y. and A.P.K. wrote the paper.

which is not enough time for the oxygenated blood to reach venules; thus, the signal is thought to originate primarily from the microvasculature (arterioles/capillaries)[8, 9, 11]. The deep cortical layer onset of hemodynamic response has been detected by two-photon microscopy[12] and similar findings have been reproduced in the human brain by BOLD fMRI[13]. The onset of the fMRI signal detected in layer 4 (L4) of the somatosensory cortex of the rat brain coincides with the major thalamocortical (TC) input[9, 10], opening the possibility that the BOLD fMRI onset corresponds to the input of neural activity across cortical layers.

To better characterize the fMRI onset with sufficient signal-to-noise ratio (SNR), a line-scanning method was implemented (Fig. 1a, details in online methods, Supplementary note 1, Supplementary Fig. 1) and applied to study laminar-specific inputs to the rat somatosensory cortex. Two saturation slices were positioned to suppress signal outside the relevant cortical area. MRI signal from the cortical area can be detected with a clear border defined by the saturation slices. The frequency-encoding-gradient was set parallel to the radial axis of the cortex and the phase-encoding-gradient was turned off so that the MRI signal along the phase-encoding-gradient is integrated into a line profile across the cortical depth (Supplementary Fig. 1a–c). Slice selection during radio-frequency (RF) excitation along with the saturation slices ensured that the signal comes from the relevant cortex (Supplementary Fig. 1d). Acquiring the line-scanning data as a function of time allowed the fMRI signal to be sampled with 50 ms temporal resolution and 50 μm spatial resolution across cortical layers from the surface to the white matter (Fig. 1b). The slice thickness used was 1–1.2 mm and the cortical space between two saturation slices was 1.0–1.5 mm, leading to a nominal resolution of 1–1.2×1.0–1.5(mm)×50(μm).

To test whether the laminar origin of the fMRI signal is determined by neural input projections or reflects the underlying distribution property of cerebral vasculature[14], we chose two neural circuits that are well studied in the rat: the thalamocortical (TC) input to the forepaw somatosensory cortex (FP-S1) and the somatomotor corticocortical input to the motor cortex (MC) of rats. Neural activation at the FP-S1 as detected by fMRI occurs through the major ascending TC input after stimulation of the forepaw. Activation of the MC detected by fMRI occurs through somatomotor connections from the barrel cortex (BC) to the MC after stimulation of the whisker pad (Supplementary Fig. 2). Using the line-scanning approach, we detected distinct fMRI onset profiles in the two circuits after stimulation: an early fMRI onset peak at L4 in the FP-S1 and two distinct onset peaks corresponding to the somatomotor inputs into L2/3 and L5 of the MC (Fig. 1b). The neural input layers can be traced by Manganese-enhanced MRI (MEMRI) *in vivo*[15, 16], and using this approach we were able to detect an Mn-enhanced signal primarily located at L4 corresponding to the TC inputs into the FP-S1 and two-bands at L2/3 and L5 in the MC corresponding to somatomotor connections (Fig. 1c). Polynomial fitting of the first significant (2 times the standard deviation) fMRI activation signal after the stimulus onset across the cortical depth determined the fMRI onset time and corresponding laminar location (Fig. 1d, e). Onset times were: FP-S1, 0.72±0.03 s (n=8); MC, 0.88±0.03 s and 0.94±0.05 s (n=7). Onset locations were FP-S1, 0.67±0.03 mm; MC, 0.42±0.01 mm and 1.01±0.03 mm. These onset locations agree with the neural input location measured by the

Mn-enhanced signal (Fig. 1, Supplementary Table 1). Therefore, the location of fMRI onset matches well with the input layers detected by Mn-enhanced peak signal across the cortical depth, and can be used to locate the source of neural inputs.

We then studied if the fMRI onset shifts when neural inputs change during cortical plasticity. We have previously mapped plasticity events by BOLD fMRI using a rat model in which plasticity is induced by unilateral infraorbital nerve resection in 4-week old animals (IO rats) [16]. In this model, two weeks after peripheral denervation, the stimulation of the intact whisker pad led to increased bilateral fMRI activation in the BC of the IO rats (Fig. 2a), whereas in the control rats with sham surgery (sham rats), the stimulation of the whisker pad activated the contralateral BC but not the ipsilateral BC (Supplementary Fig. 3a)[16]. This ipsilateral BC fMRI activation provides a good model to analyze fMRI onsets due to plasticity. The callosal projections connecting the two hemispheres mediate the ipsilateral fMRI activation in the plasticity model as determined by ablation experiments (Supplementary note 2, Supplementary Fig. 3b, c)[17, 18].

Using the line-scanning approach, we studied the onset pattern of ipsilateral fMRI activation in the deafferented BC in IO rats, and compared the response to the unaffected contralateral BC. The early fMRI onset peak in the contralateral BC of IO rats was located at the level of L4 in the same laminar position as detected in sham rats (Supplementary Fig. 4). In the deafferented BC, the fMRI onset shifted to L2/3 and L5 (Fig. 2b). Mn-tracing was used to confirm the shift in the inputs (Fig. 2c). Polynomial fitting showed that the early fMRI onset peak (0.66±0.02 s) in the contralateral BC was located at a cortical depth of 0.70±0.03 mm, corresponding to TC inputs into L4. The ipsilateral fMRI activation had two onset peaks with one peak at 0.69±0.04 s at 0.44±0.02 mm cortical depth, and the other at 0.70±0.03 s at 1.03±0.03 mm cortical depth, corresponding to callosal inputs to L2/3 and L5 (Fig. 2d, e, Supplementary Table 1). Furthermore, the strength of the callosal connections can be estimated by measuring the MEMRI signal in L2/3 and L5 plotted as a function of time after the injection of the Mn^{2+} tracer (Supplementary note 2)[16]. The slope of Mn^{2+} tracing at both layers was significantly higher in IO rats than in sham rats (Supplementary Fig. 5, $p=0.004$), indicating that the callosal circuit was strengthened in the IO rats. Taken together, the coincidence of the fMRI onset signal in the ipsilateral cortex with callosal input layers and the increase in Mn^{2+} tracing through the callosal input indicates that callosal inputs are likely to contribute to the plasticity detected. This result also confirms that the early fMRI onset can shift locations in the same cortical area due to plasticity.

It might be expected that cortical layers with stronger fMRI activation would be first to reach a statistically significant onset leading to a correlation of onset with peak fMRI. This would confound the interpretation that the laminar location of fMRI onset coincides with neural inputs. To determine this, we acquired high SNR fMRI data using the line-scanning technique and performed extensive averaging across stimulation trials. Using this approach, we were able to show that the fMRI onset profiles did not change after increasing the number of averages (Supplementary Fig. 6). We then compared the peak fMRI signal profile to the fMRI onset times across cortical layers. In both the FP-S1 and MC paradigms, the peak fMRI signal was located in superficial layers (<0.2 mm cortical depth) and was 2–3 times higher in magnitude than that in the deeper cortical layers (Supplementary Fig. 7). The

earliest fMRI onsets were located 0.3–1.2 mm deep, depending on the neural circuit mediating activity. The baseline noise level was similar across the 0.3–1.2 mm cortical depth, as was the peak fMRI response (Supplementary Fig. 7, 8). This result indicates that the location of the earliest fMRI signal was independent of the baseline noise and peak fMRI response. Furthermore, the laminar locations of the earliest fMRI onset were also consistent independent of normalization strategy (Supplementary Fig. 9–14) or if the full hemodynamic response function was used to determine the onset time (Supplementary Fig. 15–17). Cortical layers deeper than 1.4 mm had a small fMRI response. It is possible that the small fMRI signal might lead to an underestimation of the fMRI onset. However, even in the deep cortical layers, the line-scanning fMRI data were acquired in a regime that the onset time was not dependent on the SNR. Together these results point to the fact that the early fMRI onset signal does not depend on the peak fMRI response. Previously, it has been shown that it takes over a second after stimulation for the oxygenated blood to transfer from the arteries through the capillary bed to venuoles in the rat cortex [9, 10, 12]. In contrast, the early fMRI onset signal starts before the venuole BOLD fMRI response and, therefore, likely comes from the microvasculature (arterioles and capillaries)[10]. Given the timing of the responses, the fMRI onset signal likely corresponds to hemodynamic changes in the microvasculature whereas the peak fMRI signal corresponds to the delayed, venous response.

A number of studies demonstrate that neural events, on the order of 100 ms, can be separated using the BOLD hemodynamic response[19]. However, the propagation of neural activity, on the order of 5–15 ms, remains challenging to extract from fMRI signals given the temporal resolution of hemodynamic responses. In the rat barrel cortex, TC neural signals propagate from the L4 across the cortical column in less than 5 ms[20] and the transhemispheric neural signal propagates in ~12 ms[21]. The latency of fMRI activation detected in the present study is ~0.5–0.8 s following neural activity. Therefore, it is not clear how the long-lasting fMRI signal onset laminar location coincides with the neural input. The underlying mechanism of this laminar coincidence between fMRI onset and neural input remains an open question. One possibility is that the onset of the hemodynamic response follows neural firing, i.e. first-to-fire leads to first-to-dilate. This requires a mechanism that precisely orders neural firing events and the hemodynamic onsets that follow. Another possible explanation could be that neurons receiving direct neural inputs are most reliably time-locked to the stimulation at the appropriate cortical input layers[20, 22, 23]. It has been shown that TC inputs lead to the synchronous activity of L4 neurons[24] and that whisker stimulation can elicit highly time-locked neuronal responses in the sensory input projection layers of MC[23]. In our fMRI experiments, it could be that neurons directly receiving input activity are highly time-locked following each stimulus repetition. This leads to a faster and more coordinated vascular response than in layers where neurons receive propagating and temporally dispersed activity along the cortical column. A third possible explanation is that the input activity may drive the early events of neurovascular coupling that initiate vasodilation in the cortex in parallel to initiating neuronal transmission. This would mean a distinct and direct role of neural inputs on the microvasculature. Using optogenetics to activate distinct neurons at different cortical locations may provide a strategy to allow testing of these different mechanisms. It is clear that more effort will be needed to

understand the detailed neurovascular coupling mechanism at the earliest time points after neural activation to understand why the fMRI onset coincides with neural inputs.

Online Methods

MRI image acquisition

All images were acquired with an 11.7 T/31 cm horizontal bore magnet (Magnex), interfaced to an AVANCE III console (Bruker) and equipped with a 12 cm gradient set, capable of providing 100 G/cm with a rise time of 150 μs (Resonance Research). A custom-built 9 cm diameter quadrature transmitter coil was placed in the gradient. Surface receive-only coils were used during image acquisition.

Echo-planar Imaging (EPI) fMRI—For functional mapping, the fMRI was first setup with shimming, adjustments to echo spacing and symmetry, and B_0 compensation. A 3D gradient-echo, EPI sequence with a 64 × 64 ×32 matrix was run with the following parameters: effective echo time (TE) 16 ms, repetition time (TR) 1.5 s, bandwidth 170 kHz, flip angle 12°, FOV 1.92 × 1.92 × 0.96 cm^3. A block design stimulation paradigm was used. Each scanning trial consisted of 320 dummy scans to reach a steady state, followed by 20 scans with stimulation off and 10 scans with stimulation on (repeated 3 times). A total of 110 scans were performed for each trail and 6–8 trials were acquired for each rat. Electrical stimulation was described in our previous study[16]. An isolated stimulator (A360LA, WPI) supplied 2.5 mA, 300 μs pulses repeated at 3 Hz to the whisker pad and/or forepaw upon demand.

Line-scanning fMRI—A 2D FLASH sequence (TE 10 ms, TR, 50 ms, bandwidth at 5 k, flip angle 25°, slice thickness: 1.2 mm for the barrel cortex (BC) and the forepaw somatosensory cortex (FP-S1), 1.0 mm for the motor cortex (MC); FOV alignment angle to the midline: 50° for the BC, 25° for the FP-S1, and 10° for the MC) was modified to perform the ultrafast line-scanning. The phase-encoding gradient was turned off and frequency encoding gradient was set to cover a 3.2 mm line from the cortical surface into the subcortical region. Two saturation slices were set to circumvent 1.5 mm width for the BC and FP-S1, and 1 mm for the MC. The position of relevant cortices was first located by the 3D EPI fMRI. The central position of each cortex was further located based on land marking the anterior commissure (AC), with the following parameter: FP-S1 (AC 0.9 mm, lateral, 4.0 mm), BC (AC -2.4 mm, lateral, 5.4 mm), MC (AC 2.1 mm, lateral, 2.5 mm). Two block design stimulation paradigms were applied for the line-scanning study. The forepaw stimulation experiment consisted of 60 dummy scans to reach steady state; followed by 20 pre-stimulation scans, 20 scans during electrical stimulation, and 240 scans post-stimulation (total 14 second for each on/off stimulation experiment). The whisker pad stimulation experiment consisted of 60 dummy scans to reach steady state; followed by 20 pre-stimulation scans, 40 scans during electrical stimulation, and 260 scans post-stimulation (total 16 second for each on/off stimulation experiment). Each trial repeated the on/off block design paradigm for 120 times (total 28/32 min) and 6–8 trials were acquired for each rat.

To better implement the line-scanning fMRI method for future applications, it is necessary to pay attention to several issues. The line-scanning FOV should be perpendicular to the

cortical surface of interest. The curvature for a given cortical surface can influence the accuracy to determine the cortical surface from the line profiles (detail discussed in the imaging processing and statistical analysis). In this present study, the line profile through 2 mm of cortical depth was analyzed to cover the cortex from the surface to the white matter. Each cortical layer is defined based on its cortical depth location so that variation in thickness from different cortices does not influence the estimation of the neural input layers. The line-scanning technique allows extensive averaging of the data to acquire high SNR fMRI signal. The data acquired were in a regime where the onset time did not change with increasing SNR (Supplementary Fig. 6). Multiple imaging processing strategies were implemented to determine the earliest fMRI onset cortical location to ensure results were robust independent of processing strategy (detail discussed in the imaging processing and statistical analysis).

Manganese-enhanced MRI (MEMRI)—For the Mn^{2+} tracing study, a Magnetization Prepared Rapid Gradient Echo (MPRAGE) sequence was used. Sequence parameters, such as optimal inversion delay time for best tissue contrast with the MPRAGE sequence, were determined from the T_1 values obtained from a previous study[15]. Sixteen coronal slices with FOV=1.92 × 1.44 cm, matrix 192 × 144, thickness=0.5 mm (TR=4000 ms, Echo TR/TE=18/4 ms, TI=1000 ms, number of segments=4, Averages=8) were used to cover the area of interest at 100 μm in-plane resolution with a total imaging time of 44 min. For the purpose of cross-subject registration and cortical surface alignment, anatomical images (FLASH sequence) were also acquired in the same orientation as that of the MPRAGE images with the following parameters: TR=500 ms, TE=4 ms, flip angle 45°, in-plane resolution 100 μm.

Animal preparation for fMRI and MEMRI

All animal work was performed according to the guidelines of the Animal Care and Use Committee and the Animal Health and Care Section of the National Institute of Neurological Disorders and Stroke, National Institutes of Health (Bethesda, MD, USA). The infraorbital denervation procedure has been described previously[16]. Briefly, 4 week old male Sprague-Dawley rats were anesthetized with isoflurane. The infraorbital branch of the trigeminal nerve was stretched from the infraorbital foramen and up to 2–3 mm distal to the ligature was cauterized towards the vibrissal roots. For those undergoing a sham procedure, incisions were made but nerve bundle ligation and cauterization was not performed. For the IO +ablation rat group, in addition to the IO surgery, the barrel cortex contralateral to the intact whisker pad was ablated. For the cortical ablation procedure, a burr hole was drilled above the barrel cortex and an electrode was positioned 1 mm deep in the cortex. The cortex was ablated by delivery of AC current at 1 mA for 8 s using a Precision Instruments stimulator (A360LA). Rats were allowed to recover for 14–18 days before MRI imaging. A total of 84 rats including 19 naïve rats, 30 sham rats, 31 IO rats, and 4 IO+ablation rats were used (details in Supplementary Table 2). The number of animals for each experiment was determined based on our previous work to estimate the potential variance and effect size of fMRI signal or Mn-enhanced signal changes across animals[10, 16]. Data were excluded from the pool only when a rat dies were dead during MRI or Mn injection led to large internal bleeding in the brain detected by MRI.

For fMRI experiments, rats were initially anesthetized with 2% isoflurane, orally intubated and mechanically ventilated (SAR-830/AP, CWE Inc). Plastic catheters were inserted into the right femoral artery and vein to allow monitoring of arterial blood gases and administration of drugs. After surgery, all rats were given an i.v. bolus of α-chloralose (80 mg/kg) and isoflurane was discontinued. Anesthesia was maintained with a constant infusion of α-chloralose (26.5 mg/kg/hr). The rats were placed on a heated water pad to maintain rectal temperature at ~37°C while in the magnet. End-tidal CO_2, rectal temperature, tidal pressure of ventilation, heart rate, and arterial blood pressure were continuously monitored during the experiment. Arterial blood gas levels were checked periodically and corrections were made by adjusting respiratory volume or administering sodium bicarbonate when required to maintain normal levels. An i.v. injection of pancuronium bromide (4 mg/kg) was given once per hour to eliminate motion artifacts.

For MEMRI experiments, 200 nl of 50 mM $MnCl_2$ solution in 0.9% saline was injected into the barrel cortex (Bregma −2.5 mm, lateral −4.8 mm, and ventral 2.0/3.0 mm, offset 1.25 mm, tilt 4°) to trace the somatomotor and callosal corticocortical projections and 250 nl of the same $MnCl_2$ solution was injected into thalamus (Bregma −3.0 mm, lateral − 3.0 mm, and ventral 5.5 mm) to trace the TC projections. For stereotactic injections, animals were initially anesthetized by isoflurane. A small bur hole was drilled after exposing the skull. A homemade glass injection needle was placed at the proper coordinates in the stereotactic frame. Injections were performed slowly over 5–6 min using a microinjector (Cole-Parmer) and the needle was slowly removed after being kept in the injection site for 10 min after ending the injection. MRI was performed right after stereotactic injections to make sure $MnCl_2$ was delivered to the proper site. MRI was performed at 5–6 h post-injection for TC tract tracing, at 9–10 h post-injection for BC-to-MC tract tracing, and at 21–22 h post-injection for BC-to-BC transcallosal tract tracing. To measure the Mn transport as a function of time, MRI was performed at 1 h, every hour between 9–15 h, and 22 h after injection. For MEMRI, rats were anaesthetized with 1–2% isoflurane using a nose cone and rectal temperature was maintained at 37±1°C by a heated water bath. The rats were allowed to recover after surgery. All rats were free to roam and to get food within their cages, and they were kept hydrated before imaging.

Imaging Processing and Statistical Analysis

EPI-fMRI data analysis was performed using Analysis of Functional NeuroImages (AFNI) software (NIH). Detailed description of the processing was provided in a previous study[10].

The line-scanning fMRI data were stored in k-space format. Using IDL software, a fourier transform of the k space data give the cortical line profile as a function of time (Supplementary Fig. 1a). By plotting the magnitude intensity of fMRI signal along the frequency encoding direction (64 points with 50 μm resolution), the cortical surface was determined using the edge position at half the maximum signal intensity for each animal (Supplementary Fig. 1b). A fMRI percentage map was calculated by normalizing the mean baseline signal of the time series to zero (Supplementary Fig. 1c). $SI_{percentage}=(SI_i-SI_{base\text{-}mean})/SI_{base\text{-}mean}$ (i=0:0.05:15 s, SI, signal intensity, $SI_{base\text{-}mean}$, the averaged pre-stimulation SI from 0 to 1 s).

Using Matlab, the onset time of the line-scanning fMRI signal was determined. First, the standard deviation (s.d.) of the baseline signal at different depth was computed and the noise level was consistent across the cortex (Supplementary Fig. 8). The higher s.d. at the cortical surface was most likely due to vascular partial volume contribution and edge effects. The fMRI onset time was defined at the time point when the fMRI percentage increases were higher than two times (2x) the s.d. of baseline noise since this is the 95% confidence level. We plotted the onset time as the function of cortical depth to estimate the fMRI onset time profile for different cortices. The fMRI onset profile was fit with a higher order polynomial function (10^{th}–12^{th} orders) to determine the cortical position of the earliest onset times (Supplementary Table 3–4). The R^2 value for each fit is listed in the Supplementary Table 5. The onset time profiles did not change when applying the mean s.d. of the baseline noise vs. the individual s.d. for each depth of the cortex except for the cortical surface (Supplementary Fig. 9). Given the highly consistent s.d. across the cortical depth, we used two times the mean s.d. as a uniform threshold to report the onset time and cortical location in the main text. In addition, the onset time profile was also plotted with thresholds at different levels of s.d. (Supplementary Fig. 10–14,1x, 1.5x, 2x, 3x, 5x). To determine the onset time location with 1x and 1.5x s.d. thresholds, we applied clustering criteria to rule out the time points above the threshold due to noise. To analyze the effect of the SNR on the determination of the fMRI onset, the noise level of the baseline signal was plotted as a function of the number of averages. The fMRI onset times were determined based on two times the mean s.d. detected at different number of averaging. After 240 averages (two trials), the noise level, as well as the onset times, do not change with increasing SNR (Supplementary Fig. 6).

The peak fMRI signal percentage changes were plotted to compare with the fMRI onset profile as a function of cortical depth (Supplementary Fig. 7). The result clearly demonstrates the dissociation between the peak fMRI signal and the onset time. To further test whether the peak fMRI laminar profile or the potential for different hemodynamic response functions across the cortical depth contributes to the fMRI onset profile, two other processing strategies were used. First, we compared the onset time profile from the line-scanning percentage maps with or without peak fMRI signal normalization across different cortical depths. $SI_{peak\_norm.} = SI_{mean\text{-}peak} * (SI_j / SI_{j\text{-}peak})$ (j=0:0.05:2 mm, SI, signal intensity, $SI_{mean\text{-}peak,}$ the averaged $SI_{j\text{-}peak}$ from different cortical depth).

The s.d. of the baseline signal after peak normalization was plotted as a function of the cortical depth, showing the higher normalized s.d. in the deep cortical layers due to its lower fMRI peak value (Supplementary Fig. 8). To quantify the onset time of the peak normalized fMRI percentage maps, we applied multiple (1x, 1.5x, 2x, 3x, 5x) of the mean s.d. as uniform thresholds to compare the onset time profiles of the data with or without peak normalization (Supplementary Fig. 10–14). The line profiles acquired from the original data and the peak normalized data showed similar onset values (Supplementary Table 3–4).

A second strategy was to determine the fMRI onset profile based on the full hemodynamic response function. A two-gamma-variate fitting process was used to estimate the onset time for each cortical depth from the averaged and normalized fMRI percentage maps[25, 26].

$F(t)=a*(t/(p*q))\hat{}p*\exp(p-t/q)-b*(t/(r*s))\hat{}r*\exp(r-t/s)$ (t is the variable; a, p, q, b, r, s are the coefficients for two-gamma-variate-function)

Two-gamma-variate function with optimized coefficients was fitted to the normalized time courses at different cortical depths (Supplementary Fig. 15). The R^2 value for each individual fitting was plotted for different cortices, showing an excellent goodness-of-fit. The surface fitting contour of different cortices clearly demonstrated the onset laminar location varies at different cortical depth and is independent of the peak fMRI signal (Supplementary Fig. 16, 17). The onset time was estimated as the root of the two-gamma-variate function when the signal starts to increase (Supplementary Table 3–4). The results from both strategies indicate that the onset time is not associated with the peak fMRI signal across the cortical depth and the conclusion about location of onset time did not depend on the specific processing strategy.

An inconsistent finding in the fMRI literature on the hemodynamic response function is whether there is an initial decrease in BOLD signal prior to an increase[27, 28]. In a few cases of the present study, an initial dip was observed in the superficial cortical layers; however, this did not reach statistical significance in the group averages. This effect was small and inconsistent across animals. This is consistent with previous studies[8, 9, 29]. A recent fMRI study detected a small but significant initial dip with the largest affect at the surface cortical layer[12]. The reasons for only occasionally detecting an initial dip at the cortical surface in the present studies are not clear and may be due to the fluctuations of the oxygenation level of hemoglobin in the large surface vessels or partial volume effects near the surface.

The MEMRI data were analyzed by extracting the Mn-enhanced cortical line profile from MPRAGE images. For each animal, both anatomical images (FLASH) and MPRAGE images were acquired at the same geometrical 3D orientation. The MPRAGE image (MEMRI) was superimposed with the FLASH anatomical image. By analyzing the line profile across the cortex of the FLASH image, the cortical surface was determined as the position where half the maximum signal intensity was detected through the transition from skull and cerebrospinal fluid (low signal) to cortex (high signal) (Supplementary Fig. 18). The Mn-enhanced signal was plotted across the 2 mm cortical depth at 100 μm intervals. Each data point from the 100 μm cortical depth was averaged from 500 μm wide band. The Mn-enhanced line profiles of the FP-S1, MC and BC were acquired based on the line across the central position of each cortex, which was used to position the line-scanning FOV: FP-S1 (AC 0.9 mm, lateral, 4.0 mm; alignment angle to the midline, 25°), BC (AC −2.4 mm, lateral, 5.4; alignment angle to the midline, 50°), MC (AC 2.1 mm, lateral, 2.5 mm; alignment angle to the midline, 10°). The location of the Mn-enhanced peak signal was determined through the cortex and was reported as the mean cortical depth ± standard error (mean±s.e.m., Supplementary Table 1). The cortical depth of Mn-enhanced peak signal was used to determine the neural input layers. These neural input layers were compared with the fMRI onset laminar location estimated by line-scanning fMRI (Supplementary Table 1, p value was calculated by Student's t-test with two tails)). In Figure 1e and 2c, the different neural inputs layers (L4, L2/3 and L5) were determined by MEMRI. These neural input layers were defined as ~200 μm band centered at the location of the peak MEMRI signal, which was two times standard deviation of the spatial variation of Mn-enhanced signal peak

location across subjects. Paired Student's t-tests (two tails) were used to compare the mean fMRI onset times between each input layer.

MEMRI was used to characterize the strength of the callosal circuit after the Mn injection into the intact BC of the IO rats. The Mn-enhanced tract tracing signal at the L2/3 and L5 of the ipsilateral BC and contralateral MC to the injection side was analyzed in both IO and sham rats. The peak signal was extracted for quantitative analysis from the Mn-enhanced line profile. Again, each data point was averaged from 500 μm wide layers covering two consecutive slices at the center of BC (AC −2.4 mm, lateral, 5.4 mm) and MC (AC 2.1 mm, lateral, 2.5 mm). For each rat, the peak Mn-enhanced signal was located at the depth ~0.3–0.5 mm for L2/3, and ~0.95–1.15 mm for L5. The Mn injection and MEMRI imaging was done by a different experimenter who was blind to the groups of animals. Paired Student's t-tests (two-tails) were performed to compare the Mn-enhanced signal across different cortical layers between IO and sham rats.

Supplementary Material

Refer to Web version on PubMed Central for supplementary material.

Acknowledgments

This research was supported by the Intramural Research Program of the NIH, NINDS. We thank Ms. Kathryn Sharer and Ms. Nadia Bouraoud for technical support.

Abbreviations

SNR	Signal-to-noise ratio
FP-S1	Forepaw somatosensory cortex
MC	Motor cortex
BC	barrel cortex
TC	Thalamocortical
BOLD	Blood-oxygen-level-dependent
fMRI	Functional magnetic resonance imaging
MEMRI	Manganese-enhanced MRI

References

1. Ogawa S, Lee TM, Kay AR, Tank DW. Proc Natl Acad Sci U S A. 1990; 87:9868–9872. [PubMed: 2124706]
2. Biswal B, Yetkin FZ, Haughton VM, Hyde JS. Magn Reson Med. 1995; 34:537–541. [PubMed: 8524021]
3. Friston K. PLoS Biol. 2009; 7:e33. [PubMed: 19226186]
4. Moon CH, Fukuda M, Kim SG. Neuroimage. 2012; 64C:91–103. [PubMed: 22960251]
5. Menon RS, Ogawa S, Strupp JP, Ugurbil K. J Neurophysiol. 1997; 77:2780–2787. [PubMed: 9163392]
6. Chen G, Wang F, Gore JC, Roe AW. Neuroimage. 2012; 64:147–155. [PubMed: 22960152]

7. Shmuel A, Yacoub E, Chaimow D, Logothetis NK, Ugurbil K. Neuroimage. 2007; 35:539–552. [PubMed: 17306989]
8. Silva AC, Lee SP, Iadecola C, Kim SG. J Cereb Blood Flow Metab. 2000; 20:201–206. [PubMed: 10616809]
9. Silva AC, Koretsky AP. Proc Natl Acad Sci U S A. 2002; 99:15182–15187. [PubMed: 12407177]
10. Yu X, et al. Neuroimage. 2012; 59:1451–1460. [PubMed: 21851857]
11. Hutchinson EB, Stefanovic B, Koretsky AP, Silva AC. Neuroimage. 2006; 32:520–530. [PubMed: 16713717]
12. Tian P, et al. Proc Natl Acad Sci U S A. 2010; 107:15246–15251. [PubMed: 20696904]
13. Siero JC, Petridou N, Hoogduin H, Luijten PR, Ramsey NF. J Cereb Blood Flow Metab. 2011; 31:1999–2008. [PubMed: 21505479]
14. Duvernoy HM, Delon S, Vannson JL. Brain Res Bull. 1981; 7:519–579. [PubMed: 7317796]
15. Tucciarone J, et al. Neuroimage. 2009; 44:923–931. [PubMed: 18755280]
16. Yu X, et al. Neuron. 2012; 74:731–742. [PubMed: 22632730]
17. Frey SH, Bogdanov S, Smith JC, Watrous S, Breidenbach WC. Curr Biol. 2008; 18:1530–1534. [PubMed: 18848443]
18. Pelled G, Chuang KH, Dodd SJ, Koretsky AP. Neuroimage. 2007; 37:262–273. [PubMed: 17544301]
19. Lin FH, et al. Neuroimage. 2013; 78C:372–384. [PubMed: 23591071]
20. Quairiaux C, Armstrong-James M, Welker E. J Neurophysiol. 2007; 97:2130–2147. [PubMed: 17122325]
21. Shuler MG, Krupa DJ, Nicolelis MA. J Neurosci. 2001; 21:5251–5261. [PubMed: 11438600]
22. Lebedev MA, Mirabella G, Erchova I, Diamond ME. Cereb Cortex. 2000; 10:23–31. [PubMed: 10639392]
23. Chakrabarti S, Zhang M, Alloway KD. J Neurophysiol. 2008; 100:50–63. [PubMed: 18450580]
24. Bruno RM, Sakmann B. Science. 2006; 312:1622–1627. [PubMed: 16778049]
25. Cox RW. Comput Biomed Res. 1996; 29:162–173. [PubMed: 8812068]
26. Madesen M. Phys Med Bid. 1992; 37:1597–1600.
27. Uludag K. Proc Natl Acad Sci U S A. 107:E23. author reply E24. [PubMed: 20142469]
28. Buxton RB. Neuroimage. 2001; 13:953–958. [PubMed: 11352601]
29. Marota JJ, et al. Magn Reson Med. 1999; 41:247–252. [PubMed: 10080270]

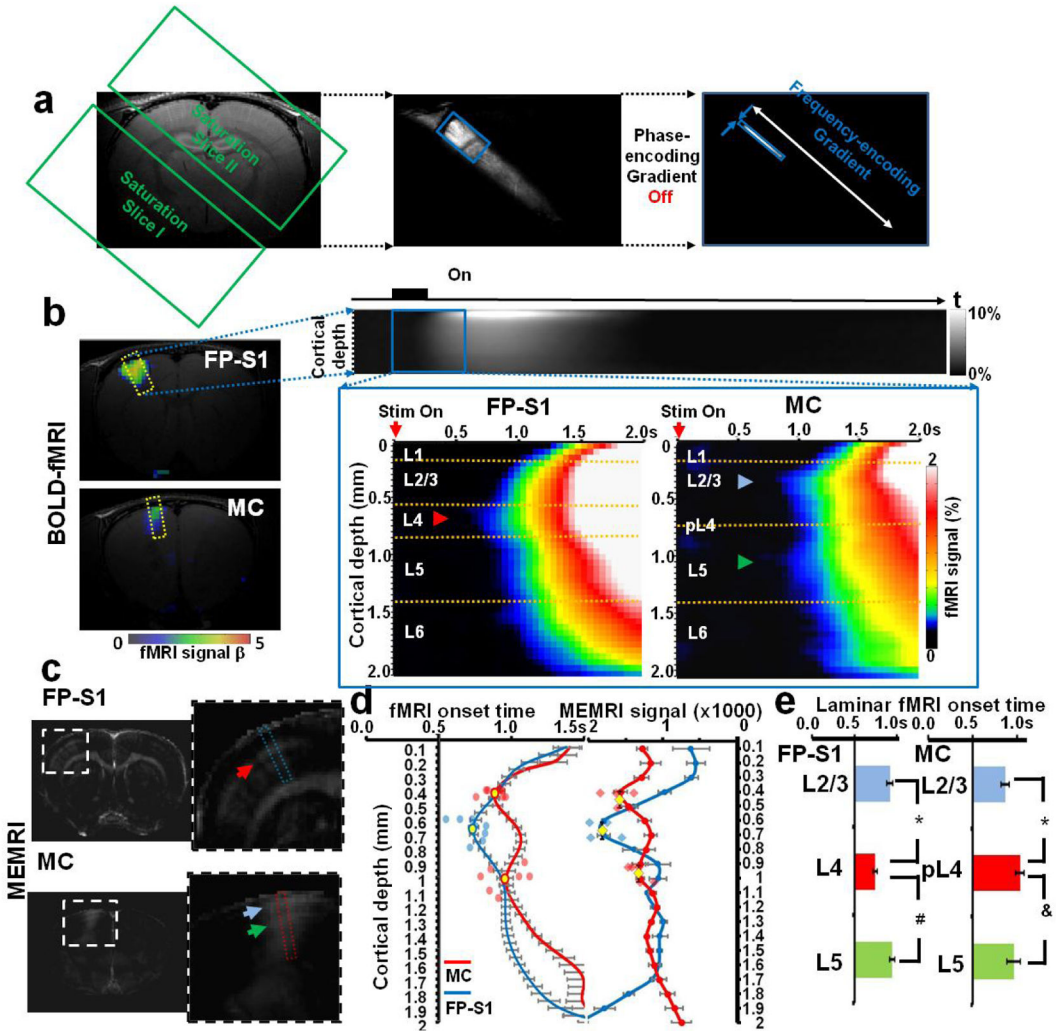

Figure 1. Characterization of the line-scanning fMRI method in rat somatosensory and motor cortex

a. The procedure to set up the line-scanning method. **b**. BOLD functional maps of FP-S1 and MC shown in the Echo-Planar-Imaging (EPI) images (left panel). The fMRI line profile was acquired from the activated FP-S1 and MC (dotted rectangular square). The stimulation paradigm was 1s off, 1s on, 13s off. An fMRI percentage change map is shown corresponding to the first events during and after the stimulus. The y axis represents the cortical depth and the x axis time. Arrowheads point to the earliest fMRI onset/s inFP-S1 (red arrowhead) and in MC (blue and green arrowheads). Red arrow represents the start of the stimulus **c**. MEMRI mapping of the TC inputs into the FP-S1 (L4, red arrow) and somatomotor inputs from the BC to the MC (L2/3, blue arrow; L5, green arrow). **d.** The fMRI onset time was determined by polynomial fitting and the Mn-enhanced signal was plotted as a function of the cortical depth. Yellow markers indicate the mean location of the earliest peak fMRI onset/s (circles) and peak Mn-enhanced signal (diamonds). Blue/red dots indicate the peak location from individual rats (FP-S1, blue, n_{onset}=8, n_{MEMRI}=4; MC, red, n_{onset}=7, n_{MEMRI}=5; error bars are ±s.e.m.). **e**. Mean onset time at L2/3, L4, and L5. Statistics were: FP-S1, * is p=0.0003 at L4 vs. L2/3 and # is p=0.0004 at L4 vs. L5 (n=8);

MC, * is p=0.001 at L4 vs. L2/3 and & is p=0.03 at L4 vs. L5. Bar graph indicates mean ±s.e.m..

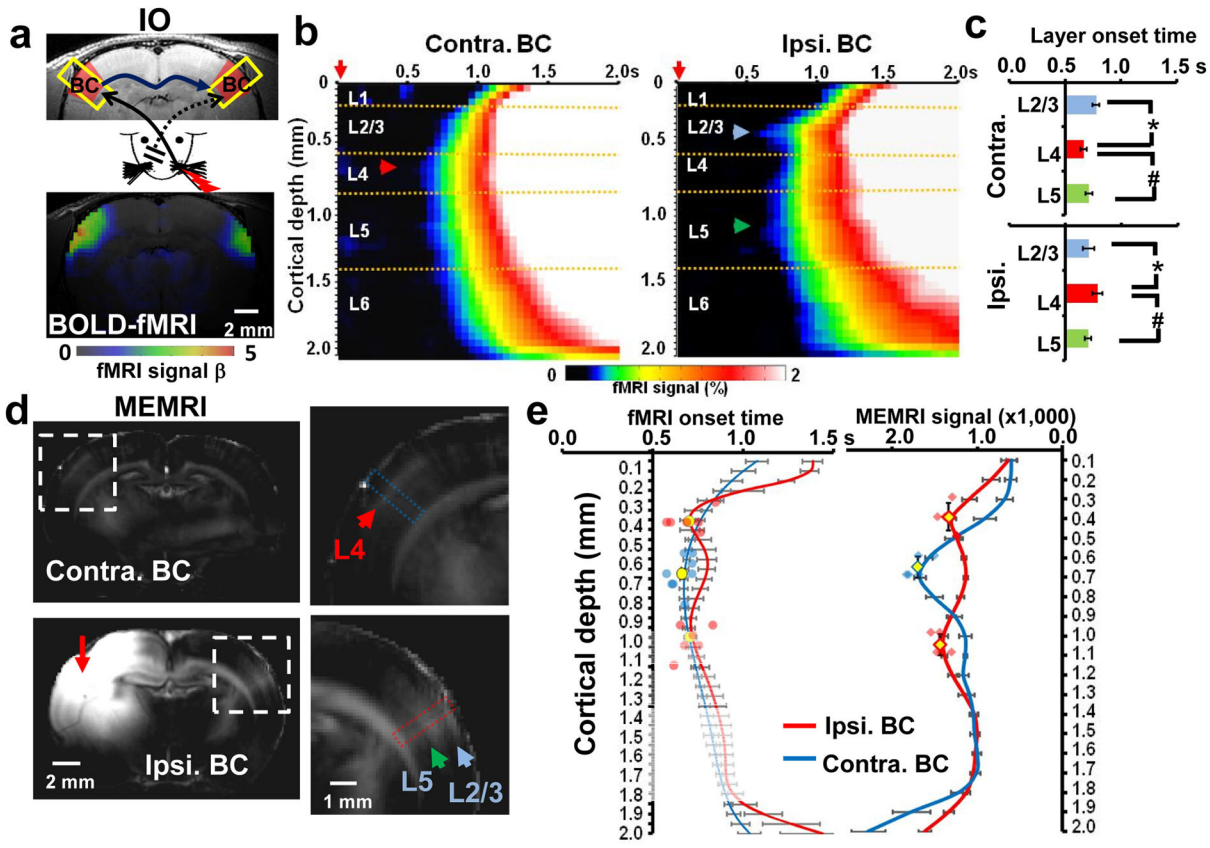

Figure 2. Mapping the inputs into the barrel cortex in a rat model of cortical plasticity

a. Schematic of the line-scanning fMRI mapping experiment in the contralateral (contra.) and ipsilateral (ipsi.) BC of IO rats. The lower panel is the bilateral fMRI activation in the BC of the IO rats with EPI-fMRI. **b.** fMRI percentage change maps in contra. and ipsi. BC of IO rats. Arrowheads point to the earliest fMRI onset signals. Contra BC (red arrowhead) and ipsi BC (blue and green arrowheads). Red arrow represents the start of the stimulus **c.** Mean onset time at L2/3, L4, and L5. Statistics were: contra. BC, * is p=0.001, # p=0.04 ($n_{contra.}$=8) and ipsi. BC, * is p=0.01, # p=0.02 ($n_{ipsi.}$=6). Bar graph indicates mean±s.e.m.. **d.** MEMRI mapping of the TC inputs into L4 (red arrowhead) of the contralateral BC and the callosal inputs into L2/3 and L5 (blue and green arrows) of the ipsilateral BC. **e**. The fMRI onset time was determined by polynomial fitting and the Mn-enhanced signal was plotted as a function of cortical depth in both contralateral (blue) and ipsilateral (red) BC. Yellow markers indicate the location of the earliest peak fMRI onset/s (circles) and peak Mn-enhanced signal (diamonds). Blue/red dots indicate the peak location from individual rats (Contra. BC., blue, n_{onset}=8, n_{MEMRI}=5; Ipsi. BC, red, n_{onset}=6, n_{MEMRI}=5; error bars are ±s.e.m.).